

Focal ratio degradation in lightly-fused hexabundles

J. J. Bryant^{1,4,*}, J. Bland-Hawthorn^{1,2}, L. M. R. Fogarty¹, J. S. Lawrence³
and S. M. Croom^{1,4}

¹ *Sydney Institute for Astronomy (SIfA), School of Physics, The University of Sydney, NSW 2006, Australia*

² *Institute of Photonics & Optical Science, The University of Sydney, NSW 2006, Australia*

³ *Australian Astronomical Observatory, PO Box 915, North Ryde, NSW 1670, Australia*

⁴ *ARC Centre of Excellence for All-sky Astrophysics (CAASTRO);*

ABSTRACT

We are now moving into an era where multi-object wide-field surveys, which traditionally use single fibres to observe many targets simultaneously, can exploit compact integral field units in place of single fibres. Current multi-object integral field instruments such as SAMI (Croom et al. 2012; Bryant et al. 2012a) have driven the development of new imaging fibre bundles (hexabundles) for multi-object spectrographs. We have characterised the performance of hexabundles with different cladding thicknesses and compared them to that of the same type of bare fibre, across the range of fill-fractions and input f-ratios likely in an IFU instrument. Hexabundles with 7-cores and 61-cores were tested for focal ratio degradation (FRD), throughput and crosstalk when fed with inputs from F/3.4 to >F/8. The five 7-core bundles have cladding thickness ranging from 1 to 8 μ m, and the 61-core bundles have 5 μ m cladding. As expected, the FRD improves as the input focal ratio decreases. We find that the FRD and throughput of the cores in the hexabundles match the performance of single fibres of the same material at low input f-ratios. The performance results presented can be used to set a limit on the f-ratio of a system based on the maximum loss allowable for a planned instrument. Our results confirm that hexabundles are a successful alternative for fibre imaging devices for multi-object spectroscopy on wide-field telescopes and have prompted further development of hexabundle designs with hexagonal packing and square cores.

Key words: instrumentation: miscellaneous:hexabundles – techniques: miscellaneous – methods: observational – instrumentation: spectrographs – techniques: imaging spectroscopy.

1 INTRODUCTION

Over the past two decades, single-fibre multi-object spectroscopic (MOS) surveys have amassed large galaxy samples from which global properties and evolutionary trends have been deduced. However, a fixed angular-sized aperture fibre can give misleading results when the same sized fibre is used to observe all galaxies irrespective of their size, distance or morphology (see for example, Ellis et al. (2005)). Spatially-resolved spectroscopy is the way forward for future galaxy surveys and will lead to significant advances in our understanding of galaxies’ morphologies and evolution. While integral field units (IFUs) have been very effective in studies of individual galaxies, up until recently, the number

of objects that can be observed simultaneously is limited. Our motivation was to develop a technology that in the future can give spatially-resolved spectra of hundreds of galaxies across a field by replacing single fibres in multi-object robotic-positioners, with compact IFU devices.

To enable a large galaxy survey with resolved spectroscopy, we have developed imaging fibre bundles called *hexabundles* (Bland-Hawthorn et al. 2011). Earlier hexabundle designs were constructed by strongly fusing the fibres. This distorted the fibres, removing the interstitial holes, but at the same time significantly worsened their optical performance (Bryant et al. 2011). These bundles have been now superseded in preference for lightly-fused bundles in which the cores remain circular and have significantly better optical performance at the cost of a lower fill-fraction.

* E-mail: jrbryant@physics.usyd.edu.au (JJB)

One of the key performance criteria for astronomy is

to minimise focal ratio degradation (FRD). FRD increases the output cone half-angle θ (where $NA = \sin\theta$, and $f\text{-ratio} \sim 1/(2NA)$) of light from the optical fibre compared to the cone half-angle of light put in (also known as NA up-conversion). The main causes of FRD are due to light scattering in the fibre from irregularities and microbends, distortion of the fibre from stress, compression or tight bend radii and the quality of the fibre end finish (for a detailed discussion of the causes of FRD, see for example Haynes et al. 2011; Oliveira, de Oliveira & dos Santos 2005; Carrasco & Parry 1994). The implication of FRD is that the spectrograph either needs to be physically bigger to collect all the light from the larger angles, or there will be light lost from the system where the acceptance angle of the spectrograph is exceeded. In order to put constraints on the applications of hexabundles, we have characterised the FRD of a number of hexabundles in detail, using a range of input beam speeds used in astronomy. The hexabundles have a range of cladding thicknesses, from 1–8 μm and either 7 or 61 cores. The hexabundle tests presented here were all using AFS105/125Y fibre. The 61-core hexabundles were then employed in the Sydney-AAO Multi-object Integral field spectrograph (SAMI) (Croom et al. 2012; Bryant et al. 2012a) prototype version, before it was more recently upgraded to a new fibre type with new hexabundles.

In Section 2 we outline the testing method and describe the specifications of the hexabundles being testing. The performance of the hexabundles in terms of FRD, throughput and cross-talk is discussed in Section 3. Section 4 discusses future development and then the summary is given in Section 5.

2 DESCRIPTION OF THE HEXABUNDLE DEVICES AND TESTING METHOD

2.1 Specifications of the hexabundles tested

Five 7-core hexabundle devices were tested, each with a different cladding thickness, as well as two 61-core hexabundles (shown in Fig. 1). The 7-core hexabundles have cladding thicknesses of 1, 2, 4, 6 and 8 μm , while the 61-core hexabundles both had 5 μm cladding thickness for all cores. The fibres used in each of the bundles was low-OH AFS105/125Y with a limiting numerical aperture (sine of the maximum acceptance cone angle) of 0.22 and core and cladding diameter of 105 μm and 125 μm respectively, before the cladding was etched away over a ~ 2 cm length where the fibres were then fused. Each of the bundles has cores which are lightly fused so that the fibres are mostly circular but interstitial holes remain, giving fill-fractions (area of cores to that of the bundle) of between 0.87 and 0.67 (for 1 to 8 μm cladding thickness respectively). Beyond the fused region the individual fibres coming out of the hexabundle device have the full 10 μm cladding thickness.

2.2 Method for testing FRD, cross-talk and throughput

Fig. 2 shows the setup used to assess FRD for all of the hexabundles tested. An Oriel LED source was focussed through a filter into an SMF-28 fibre which is multimoded in the

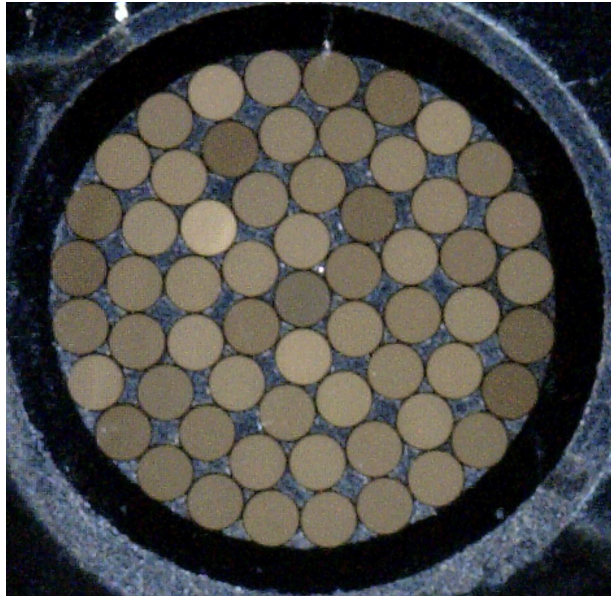


Figure 1. One of the 61-core lightly-fused hexabundles. The interstitial holes are filled with soft, low refractive index glue. The cores are 105 μm in diameter and 115 μm with cladding.

wavelength range being tested, and has an apparent core size of $\sim 10\mu\text{m}$. Two different filters were used in turn, for each measurement, and they were Bessell *B* and *R*-band filters; the *B*-band filter centred on 457 nm with a FWHM of 27 nm and the *R*-band filter centred on $\sim 596\text{nm}$ with an asymmetric profile of 60 nm width. The output of this fibre was aligned with the focus of a lens with a 75 mm focal length. An adjustable iris in the collimated beam was used to set the beam speed into the hexabundle within a range of F/3.4 to F/20. The profile of the beam going into the iris was designed to significantly overfill the iris so that the collimated beam fed through the iris to the focussing lens was just the central part of the gaussian beam from the input fibre. The result was close to a flat-topped square input function into the hexabundles (see the input curves in Fig. 3 later). The collimated beam was then refocussed by a 35 mm focal length lens to form the input beam which was fed into the hexabundles. The focussed F/3.4 input spot diameter was 50 μm (at 0.5% of the peak profile intensity) and therefore smaller than the core size to ensure no light was input into adjacent cores to contaminate cross-talk measurements. Initially an SBIG camera was used to image the input beam in the far-field. The camera was then replaced by a mount for the fused input end of the hexabundles, which was carefully aligned (see section 2.2.1 below) on axis so each hexabundle could be mounted and measured in turn.

Single fibres coming out of the hexabundles were cleaved (details of the cleave quality are discussed in section 3.1 below) and mounted on a plate that has parallel v-grooves. Each fibre was gently secured to the plate with tape, using the minimum pressure required to stop them from slipping, in order to reduce any stress on the fibre. The contribution of this method to the FRD is assessed in section 2.2.1. The v-grooves were aligned with a pair of camera lenses, which collimated and then refocussed the output light. An SBIG camera imaged the output at a precise back focus position.



Figure 2. The testing set up for measuring FRD as described in section 2.2. The input system (lower) re-images an SMF-28 fibre to form an input light cone into the hexabundle (on the far left of the lower image) with an input NA defined by the adjustable aperture. The output system (top), re-images the fibre onto the camera.

The images were dark subtracted using separate dark images, then the barycentre of the imaged spot was fitted. Encircled energy was calculated in concentric rings about the centre position using aperture photometry packages within IRAF (Tody 1986). Within the range of f-ratios being tested, both the input and output cone angles were very much less than the limiting NA of the fibre. We therefore use ‘NA’ to describe $\sin\theta$ of the cone half-angle θ . Encircled energy is measured in increasing radii on the image. The radii, when combined with the back focal distance and pixel size then gives the cone half-angle and hence output NA versus encircled energy was calculated. Total integrated counts were then compared between the core with the input light, and the surrounding adjacent cores, to assess cross-talk.

2.2.1 Errors in FRD due to alignment of the optics and positioning of the fibres

Any FRD test setup will have alignment uncertainties that lead to geometrical FRD which adds to the measured FRD of the fibre. Therefore accurate characterisation of the system errors is essential. The accuracy of the NA measurements from which FRD is assessed is significantly dependent on the alignment of the testing apparatus, and the cleave on the ends of the fibres.

There are three main contributions to the measurement uncertainties in the *input* NA or f-ratio feeding the hexabundle, and they are due to alignment. Firstly, the NA input into the hexabundle was measured using a camera in place

of the hexabundle holder. The camera was positioned on-axis on the stage used to focus the hexabundles. Any angle between the camera and the input beam will record an incorrect input NA and is apparent from fitting the spot image over the travel of the stage. The uncertainty in the input NA measurements due to the alignment of the camera to the input beam is ± 0.0005 . Secondly, positioning the fibre holder relative to the input beam introduces an uncertainty in NA into the fibre of $< \pm 0.001$. Thirdly, the accuracy with which the adjustable aperture can be set, results in an NA error of $< \pm 0.0005$.

The alignment uncertainties of the *output* optics further contribute to uncertainties in the NA measurements in the following way. The V-groove plate was aligned with the optical axis, however, there are slight angle differences depending on each fibre. This is due to *both* how the fibres sit in the v-grooves and potentially any bending of the output light by sub-1-degree variations between cleave angles from fibre-to-fibre. These errors were measured by shifting the V-groove plate back and forward and imaging the shift in each core. The resulting measured NA uncertainty was up to ± 0.004 . To test the impact of the tape holding the fibres on the plate, we applied tape firmly with repeated applications and found a maximum variation in NA of less than ± 0.002 . When lightly secured, the measurement uncertainty will therefore be $\ll \pm 0.002$. Alignment of the camera was found to give an NA uncertainty $< \pm 0.001$. The focus on a $105\mu\text{m}$ -core multimode fibre is less precise than for single-mode fibre as different modes focus at slightly different points. Coupled with any focussing errors from the optics, this results in

Table 1. Summary of the contributions to uncertainties in FRD from measured NA errors along with other percentage errors affecting throughput. All values are the maximum (not typical) uncertainties.

Alignment component	\pm max. error in NA
Input into hexabundle:	
Input beam camera alignment	0.0005
Fibre holder positioning	0.001
Input aperture repositioning	0.0005
Output reimaging optics:	
V-groove plate alignment	0.004
Securing fibre to the plate	0.002
CCD camera alignment	0.001
End face focus	$0.0067 \times \text{NA}$
Chromatic aberrations in lenses	0.0009
Other uncertainties: (%)	
Light source variability	< 1
Throughput from coupling position	$\ll 5$

an uncertainty in the NA of $\pm 0.0067 \times \text{NA}$, or ± 0.0007 to ± 0.0013 for an output NA of 0.1 to 0.2 respectively.

Table 1 summarises the errors. All uncertainties were combined in quadrature to give the measurement error, and then the profile fitting errors were included to give the total uncertainties listed in each figure (used in the calculation of output NA, NA upconversion and f-ratio errors)

Time variation in the input light intensity plus variations in the SBIG camera response, were quantified with repeated images through one core of the bundle in time periods ranging from second to hours. The maximum variation in resulting integrated counts was $< 1.0\%$ with typical values of $\sim 0.2\%$.

It is important to note that these alignment errors in any FRD test setup can introduce geometrical FRD, which can worsen the apparent measured FRD. In that sense, the measured FRD from different setups will vary, and will always be a worst case. FRD results are therefore most meaningful when compared to a bare fibre measured with the same apparatus.

2.2.2 Coupling position

If the focussed input spot is centred on a fibre, more light will couple into the central modes. However, if the input spot is significantly offset from the centre, the amount of light that gets into the fibre will be different depending on the fraction of light coupled into higher-order modes. The sensitivity of the results to the coupling position of the light into each core of the hexabundles was tested by aligning the input spot with the centre of the fibre (using a microscope) and then offsetting it from the centre to a number of positions, but still keeping the spot size entirely within the core (the spot size was $< 50\mu\text{m}$ at 0.5% of the peak intensity). The resulting variation in throughput was measured as the integrated counts from aperture photometry on the output ccd image, when the same light level was input.

The input LED light source intensity varies by 1%, while the throughput varied by up to 5%. This agrees with the results of Horton & Bland-Hawthorn (2007) who similarly found a variation of only 5% in throughput between different coupling positions within the core of multi-mode fibres. The same test on a hexabundle core found the same 5% variation in throughput due to coupling. The precision with which we could align to the centre of the fibres using the microscope, allowed a smaller centring uncertainty than the range of coupling positions tested, and we therefore expect the throughput error from coupling to be $\ll 5\%$.

3 RESULTS AND DISCUSSION

3.1 Focal Ratio Degradation (FRD)

The impact of FRD on the encircled energy curves is shown in Fig. 3. Worse FRD shifts the curve to the right because the output cone angle θ is larger, giving a larger NA for a given percentage of the encircled energy. The horizontal gap between the input and output profiles at 90 or 95% encircled energy is the NA upconversion. Worse FRD corresponds to a larger NA upconversion. For clarity, we have shown a representative range of curves, highlighting the difference between the central cores and outer cores in several typical hexabundles. As with all fibres, the FRD of the AFS105/125Y fibre is worse when the input f-ratio is higher (Fig. 3, lower row). At low f-ratios ($F/\sim 3.4$, top row), all the fibres tested demonstrated the same FRD within errors.

Repeatability of these profiles was checked by reimaging the 61-core bundle after re-centring the input spot, re-focussing, changing the input light levels, and refitting the profiles. Over 16 images taken of one core with these changes, the output NA versus encircled energy profiles were coincident within an NA scatter of only ± 0.003 .

Variability in the FRD curves can potentially come from the end cleave. The cleaves on the output of individual fibres were very carefully checked under a microscope to ensure that the cleave angle was < 1 degree and that there were no cracks or damage to the core. We ensured that the score mark from the cleave was only in the cladding and not near the core and there were no scratches or residual damage from the cleave on the core. In each case there was some surface roughness on the core which we attempted to minimise. The surface roughness was gauged from the microscope images, some examples of which are shown in Fig. 4. We tested FRD of cores with a range of apparent surface features after many re-cleaves of the same cores. We found a point at which the remaining surface features did not change the output encircled energy profiles within the errors. We therefore believe that the difference in encircled energy measurements between cores is not dominated by variations in the cleaves for the 61-core bundles. This is further confirmed by the reduced scatter at lower input f-ratio. If the cleaves strongly affected the profiles then we would see the same scatter between curves as we do at higher input f-ratios.

It is notable from Figs. 3 (e.g. black solid lines) and 5 (solid lines) that the central core of the bundles has better FRD than the outer cores. When the input f-ratio is a low value, the difference is less than the errors. However, for higher input f-ratios where the difference is more apparent, we attribute the worse FRD of the outer cores to more

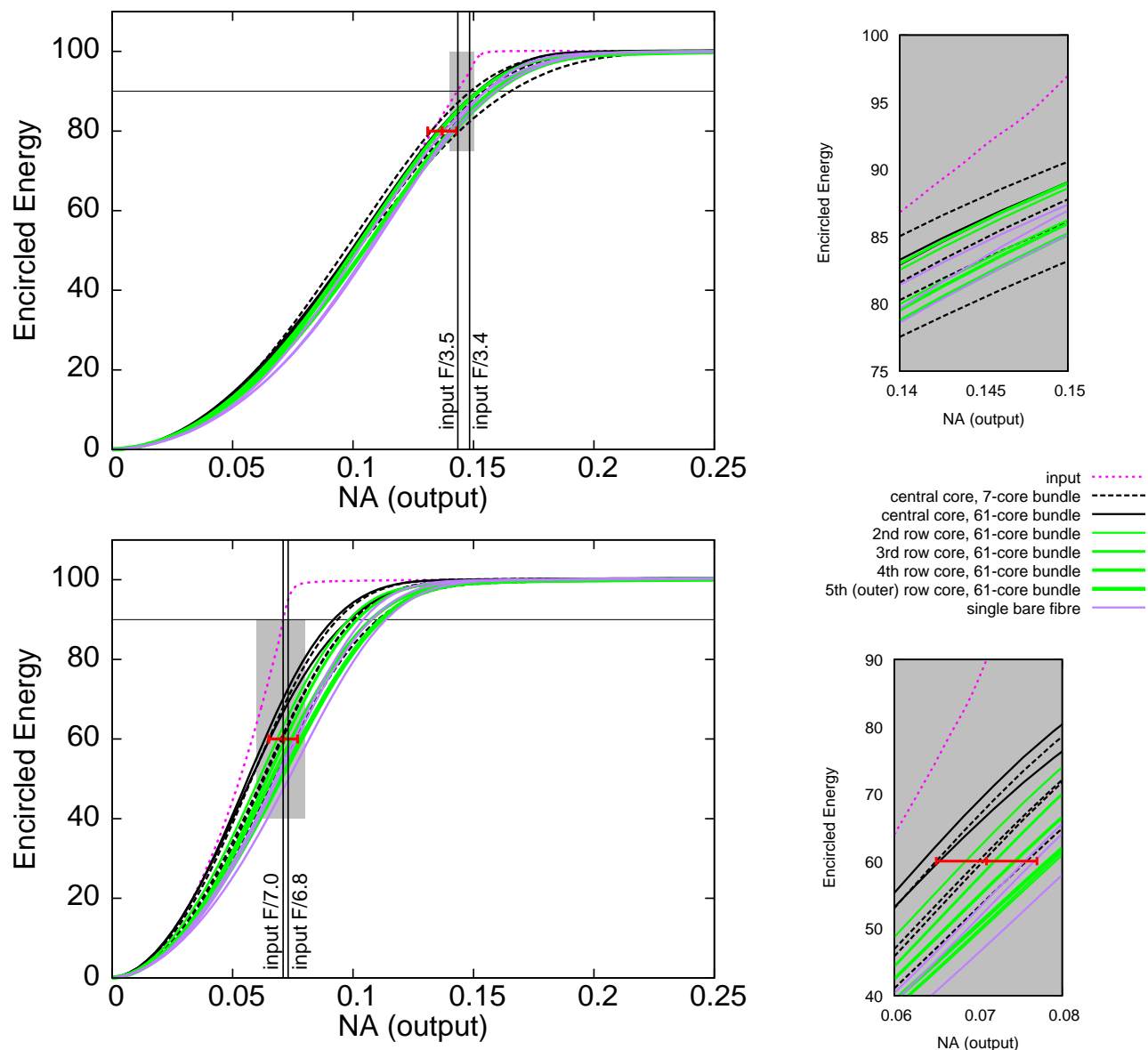


Figure 3. Encircled Energy versus Numerical Aperture ($NA = \sin\theta$; for output cone half-angle θ) profiles through the Bessel blue ($\sim 0.45 \mu\text{m}$) filter for the central cores (black) of the 7-core (dashed lines) and 61-core (solid lines) hexabundles as well as a number of the non-central cores from a 61-core hexabundle (green lines). The thickness of the green lines is proportional to how far the core is from the centre of the bundle. Grey shaded box regions are shown magnified on the right. The dotted magenta line is the input beam profile. The NA uncertainty due to alignment, focus and measurement errors is ± 0.006 as illustrated by the representative red error bar. For clarity, plots are only shown for two of the input f-ratios tested - when 95-90% of the encircled energy of the input light cone was within F/3.4-3.5 (top row), and F/6.8-7.0 (bottom row), and the equivalent NA positions for these f-ratios are marked by the vertical black lines. Purple lines are the curves for three single bare fibres that have the same AFS105/125Y fibre as the bundles. At low input F-ratio, the error bar is larger than the scatter between curves.

distortion than the central core due to the symmetry of the bundle. The outer cores are essentially circular, but even the light fusing has a small effect which can worsen the FRD and is noticeable when the input f-ratio is high.

All FRD measurements were taken with cleaved cores. The hexabundles may well perform better with polished ends or index matching gel coupling to a glass slide. In current uses of these hexabundles (i.e. in the original SAMI instrument before upgrade) the loose hexabundle fibres were spliced to much longer fibre runs that terminate in polished slit blocks. The aim was to retest the hexabundles

through these polished slit blocks, however the FRD introduced through this particular fibre run significantly degraded the FRD to make it an invalid test of the hexabundle performance. We have therefore not got a direct test of these hexabundles with polished fibres or with index matching gel and glass slides. Comparisons of these end finishing techniques have been done before by others and the results can be used to predict how much better the hexabundles may perform with different end finishing. For example, Haynes et al. (2011) (their table 4) found a 5% increase in encircled energy at F/3.6 (at 532nm) for index-matching gel

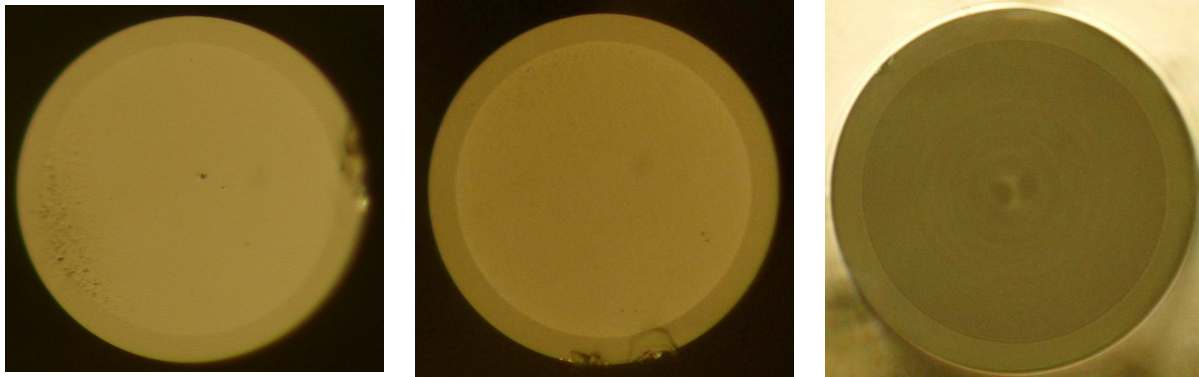


Figure 4. Microscope pictures of individual cleaved fibres at the output of the hexabundles. Typical unacceptable surface structure seen on cleaved fibre cores include a rougher surface across part of the core opposite the cleave impact point, as well as individual pits in the surface (both shown in left image). Fibres were re-cleaved to minimise these defects, to give typical core-finish shown in the centre and right images. Fibres were also re-cleaved if the cleave impact reach the core as in the central image. The right image illustrates the finish we considered acceptable.

plus glass slide compared to a good cleave. This level of improvement in Fig. 3 (top) would shift the outer encircled energy profile for the worst FRD cores to agree with the best central cores, and the best cores would be better still. Poppett & Allington-Smith (2010, their fig. 5) compared a polished end finish with the combination of a cleaved fibre plus index-matching gel. Across the range of input f-ratios we have tested, our central fibre results are similar to the polished fibre results in their fig.5 (both using 95% encircled energies). They show that cleaving and using index-matching gel improves the FRD somewhat. Therefore we assume that the performance of the hexabundle fibres when used in an instrument with index-matching gel will be at least as good as our central core results, but likely better, and the plots in Fig. 5 should be interpreted with this in mind.

The FRD was first quantified by the difference in NA between the output and input profiles at an encircled energy of 90 and 95% (NA upconversion) and was measured for input beam speeds from $F/3.4$ to $>F/20$. The result is shown in Fig. 5 (top) for $F/3.4$ to $F/8$. A second measure of FRD is how much light is lost from within the input cone angle by output. This is plotted as the percentage of the total encircled energy out of a fibre that is within the same light cone angle as the input (defined by the input f-ratio) as in Fig. 5 (middle). The third numerical quantification of FRD comes from a measure of the output angle (or f-ratio) that contains 90 or 95% of the encircled energy at each input f-ratio (Fig. 5 lower). For an input beam at $\sim F/3$, the bundles have little or no FRD as the NA upconversion and output f-ratios are (within the error bars), in agreement with the input values. In fact the FRD shown for $\sim F/3$ includes the geometrical FRD in the test equipment within the errors as discussed in section 2.2.1. Like all fibre systems, hexabundles lose less light from FRD when the input f-ratio is a low value (e.g. SAMI has $F/3.4$ input). However by $\sim F/8$, the central fibres have $\sim 64 - 69\%$ of the light from the fibre, coming out within $F/8$ (Fig. 5, middle).

In practice, fibres are used in astronomy with low input f-ratios because of the impact of FRD. It is less productive to use fibres beyond $F/8$, however, at any f-ratio, the light

loss due to FRD can be minimised with a larger acceptance cone into the spectrograph. For example, if $F/6$ is fed into the hexabundle, then $> 90\%$ of the light will go into a spectrograph that accepts an $\sim F/5$ beam for the best cores with good end finish (Fig. 5, lower left panel).

While FRD has been shown to be dependent on fibre end finish, microbends, and stresses on the fibre, the wavelength dependence of FRD is unresolved. Some studies have found no dependence (Crause, Bershady & Buckley 2008; Schmoll, Roth & Laux 2003), however Poppett & Allington-Smith (2010) found worsening FRD with increasing wavelength, but not to the extent predicted by the theoretical models of (Gloge 1972), while Murphy et al. (2008) found improving FRD with increasing wavelength. Our FRD measurements have an advantage that the two separate filters were exchanged with no change to the fibre position, cleave, mount or input NA. Therefore, the effect due to wavelength is isolated from other contributions to FRD. While the FRD at the two wavelengths overlaps within errors, the shorter wavelength is consistently worse for all fibres measured (see Fig 3 and 5). Chromatic aberrations in the input lenses have been ruled out as the cause because the effective input NA was measured separately at each wavelength and the difference found to be < 0.0009 . However, the difference in input f-ratio for a given output f-ratio in Fig 5 between colours is very much larger than this (e.g. for output of $F/4.7$ at 95% encircled energy, the difference between the red and blue input f-ratio is equivalent to an NA or 0.005, 5 times that possible from chromatic aberrations). In order to confirm the extent of the wavelength dependence, a larger wavelength range would need to be tested.

3.2 Comparison of hexabundle and single fibre results

In order to assess how the hexabundles perform compared to a single fibre of exactly the same type and length, bare AFS105/125Y fibres were mounted into an SMA connector on one end and cleaved at both ends. They were then tested in exactly the same way as the hexabundles. There were dif-

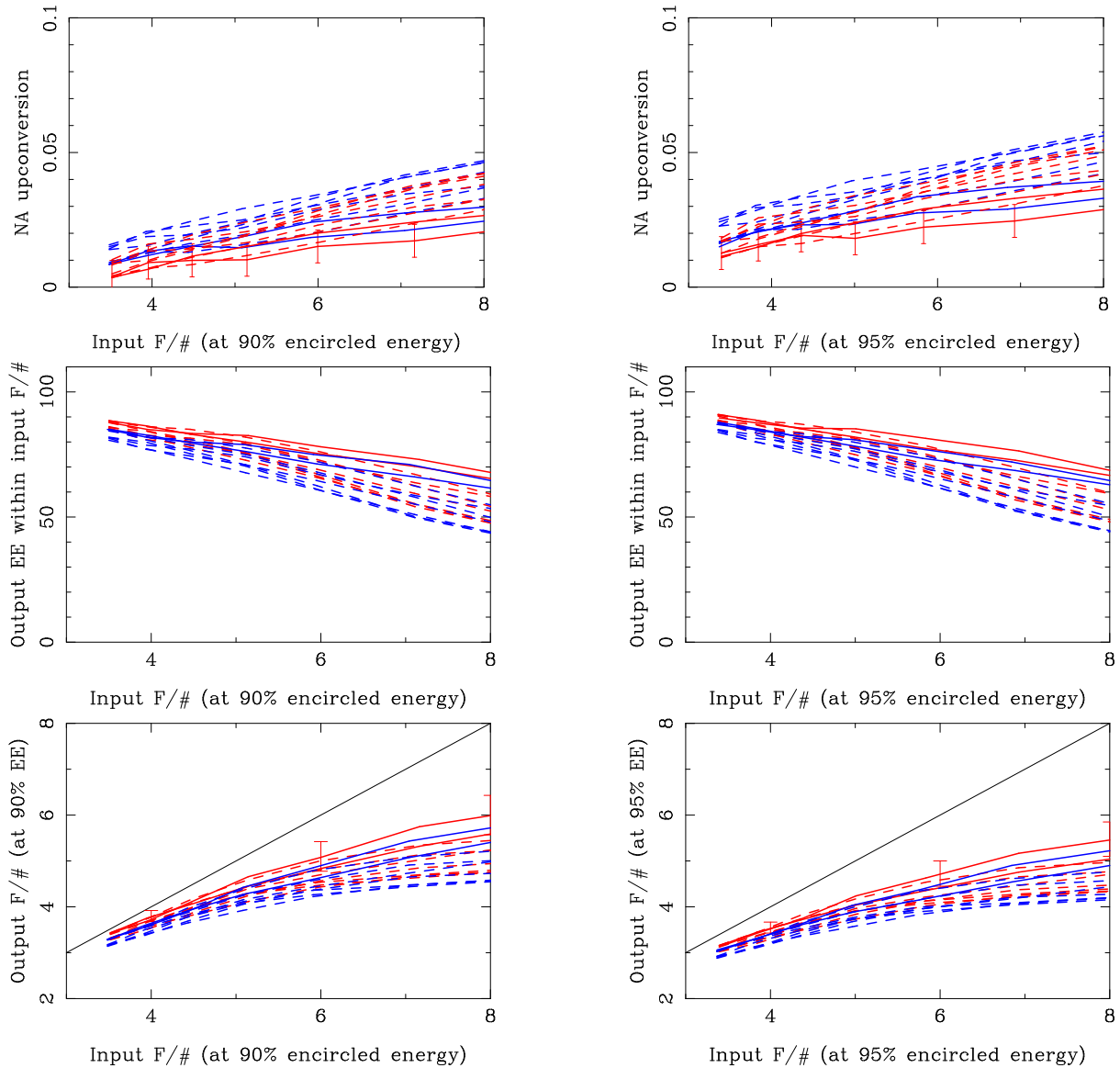


Figure 5. Focal ratio degradation results for the central core (solid lines) and outer cores (dashed lines) of two 61-core hexabundles. Each plot is shown for the case where the f-ratio is measured at 90% (left) and 95% of the total encircled energy (right). Red and blue lines are results through the Bessel R and B (~ 0.65 and $0.45\mu\text{m}$) filters respectively. *Top*: NA upconversion (difference between output and input NA or $\sin\theta$ for half-cone angles θ at 90% and 95% encircled energy) versus the f-ratio of the input beam. For clarity, the error bars are shown for one curve only, but they are representative of the uncertainties for each curve. These are the errors in the data for this core in this bundle, not the errors due to the variance between cores and bundles. *Centre*: Input f-ratio versus the percentage of encircled energy within the same f-ratio at output. *Lower*: Input f-ratio versus output f-ratio at 90/95% encircled energy. Within errors, there is no FRD at $\sim F/3$ (90% encircled energy), but FRD worsens with higher input f-ratios.

ferences between batches of bare fibre, such that the bare fibre FRD curves spanned the same range of FRD as the curves for the central and outer hexabundle curves, but repeated samples from the same batch were always consistent within the errors. For clarity, only a sample of the bare fibre curves are shown in Fig. 3 (two from the same batch, and one from a different batch). While some of the bare fibres tested had similar FRD to the best central hexabundle cores, none had less FRD. Therefore the hexabundles perform as well as bare fibre.

3.3 Cross-talk

In a hexabundle, scattering of light out of one core, may result in coupling into an adjacent core, which will then be seen as cross-talk. Thinner cladding allows more coupling of higher-order modes between cores. The measured cross-talk is given in Fig. 6. The cross-talk is $< \sim 0.5\%$ for $2\mu\text{m}$ cladding thickness and above. There is a marked increase in cross-talk for $1\mu\text{m}$ cladding, at which point the cross-talk outweighs the higher fill-fraction of 87%. However, increasing the cladding to $2\mu\text{m}$, only decreases the fill-fraction by 3%, while decreasing the cross-talk to $\sim 0.5\%$. For practical purposes the cross-talk measured here is very small com-

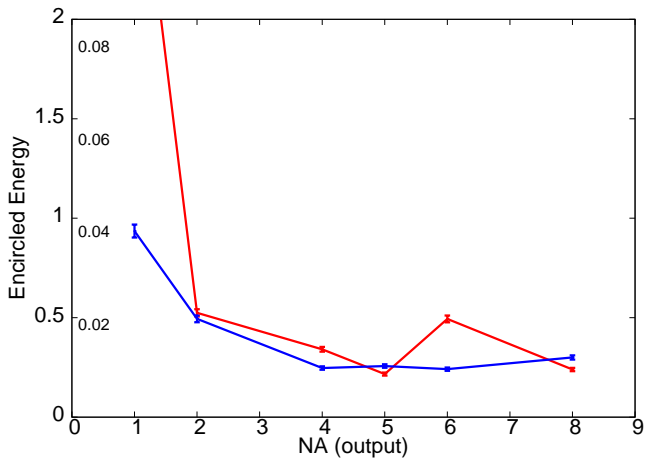


Figure 6. The % cross-talk (also given in dB inside the box) from the central fibre into all 6 surrounding fibres at F/3.4 input versus the cladding thickness of the fibres. The 7-core hexabundles have 8, 6, 4, 2 and $1\mu\text{m}$ cladding, while a representative 61-core hexabundle has $\sim 5\mu\text{m}$ cladding. The line colour represents the results through the *B* and *R*-band filters. Notice that the cross talk is insignificant at below $\sim 0.5\%$ in all but the thinnest cladding. The error bars include the light source variability and throughput variations from input coupling position.

pared to the effect of seeing. In expected uses of hexabundles, where each core is approximately the same angular size as the FWHM of the seeing disk (e.g. in SAMI), 45% of the power from the seeing disk is in the adjacent cores (and 50% in the central core). In that case, 0.5% cross-talk is negligible. The cores would need to be several seeing FWHM across for this level of cross-talk to be significant.

The cross-talk is slightly higher in the red filter compared to the blue. While the scattering model of Gloge (1972) predicts that scattering should be worse at longer wavelengths we see a much smaller effect than predicted by that model, and in fact have found the FRD to be worse in the blue. However, in the case of cross-talk, the much poorer blue throughput of the fibres most-likely has a larger impact than scattering. This is because only light travelling at a large angle to the optical axis of the fibre will be lost from one fibre into the next, and therefore the path length of that light will be larger by the time the light exits the adjacent fibre. A larger path length will suffer more absorption in the blue leading to a smaller measured output from the adjacent fibres and hence a smaller cross-talk in the blue.

3.4 Throughput

Throughput losses in individual fibres can be due to absorption in the core material or scattering of higher-order modes due to imperfections. Where that scattering leads to cross-talk, the cross-talk between fibres serves to give a loss from an individual fibre but not a systemic loss from the resultant image. Therefore, in the following throughput tests, any cross-talk (see Fig. 6) will have reduced the measured throughput by up to 1%, however this loss would be recovered in the image from a telescope.

Fig. 7 compares the throughputs of several fibres within one bundle, as well as the central fibre in 4 different bundles. Data reduction techniques applied in aperture photom-

etry were used to measure the total output counts (which is equivalent to the 100% level in the encircled energy plots in Fig 3) in order to decouple the throughput losses from FRD losses. The ratio of the output to the input counts was then corrected for the 3.3% reflection at the air/glass interface at either end of the bundle. This correction was necessary because in any astronomical instrument, the hexabundle face should be anti-reflection coated (and the test bundles were not), and the loose fibre ends will be spliced to fibres that feed directly into a spectrograph, typically coupled in with index-matching gel. Small fluctuations in the LED source, input light photometry, photometric fitting errors, errors in the assumed value for the air/glass interface reflection, and repeatability of the aperture size setting, all contributed to the total error in this throughput test.

The throughput of the fibres relative to the input light is consistent within errors, across all the input f-ratios tested. This is because at all the f-ratios shown, the effect of FRD is not substantial enough to fill the maximum NA of the fibres (see Fig. 3). Absorption is the dominant loss, and is responsible for the reduced throughput at shorter wavelengths in this AFS105/125Y fibre. It is notable that this loss was a driver behind upgrading the hexabundles and fibres used in the SAMI instrument, to a fibre type with higher throughput.

Fibre-to-fibre throughput variations within a bundle are less than the errors giving a consistent imaging bundle. Between 4 different bundles tested, the central core also showed throughput variations consistent with the fibre-to-fibre variations, indicating that there is consistency in the batches of hexabundles.

4 APPLICATIONS AND FUTURE DEVELOPMENT

The first on-sky demonstration of hexabundles was in the SAMI instrument on the Anglo-Australian Telescope (AAT), which has now seen two generations of hexabundles, starting with the 61-core models from this paper. While a number of different circular-packed hexabundle types have been made, new developments of hexabundles are focussed on increasing the fill fraction by using different packing geometries including a regular hexagonal packing of circular cores, or alternatively, using square core fibres. A discussion of the trade-offs with these geometries can be found in Bryant et al. (2012b).

The success of hexabundles has led to plans for a much larger robotically-positioned IFU instrument called HECTOR (Lawrence et al. 2012). In preparation for HECTOR, hexabundles are being tested in autonomous position robots called starbugs (Gilbert et al. 2012).

5 SUMMARY

Hexabundles have been developed with FRD and throughput performance at low input f-ratios, equivalent to that of the bare fibre they are made from. Therefore, they can replace single fibres in multi-object spectroscopy, with the advantage of spatially-resolved spectroscopy on many objects simultaneously.

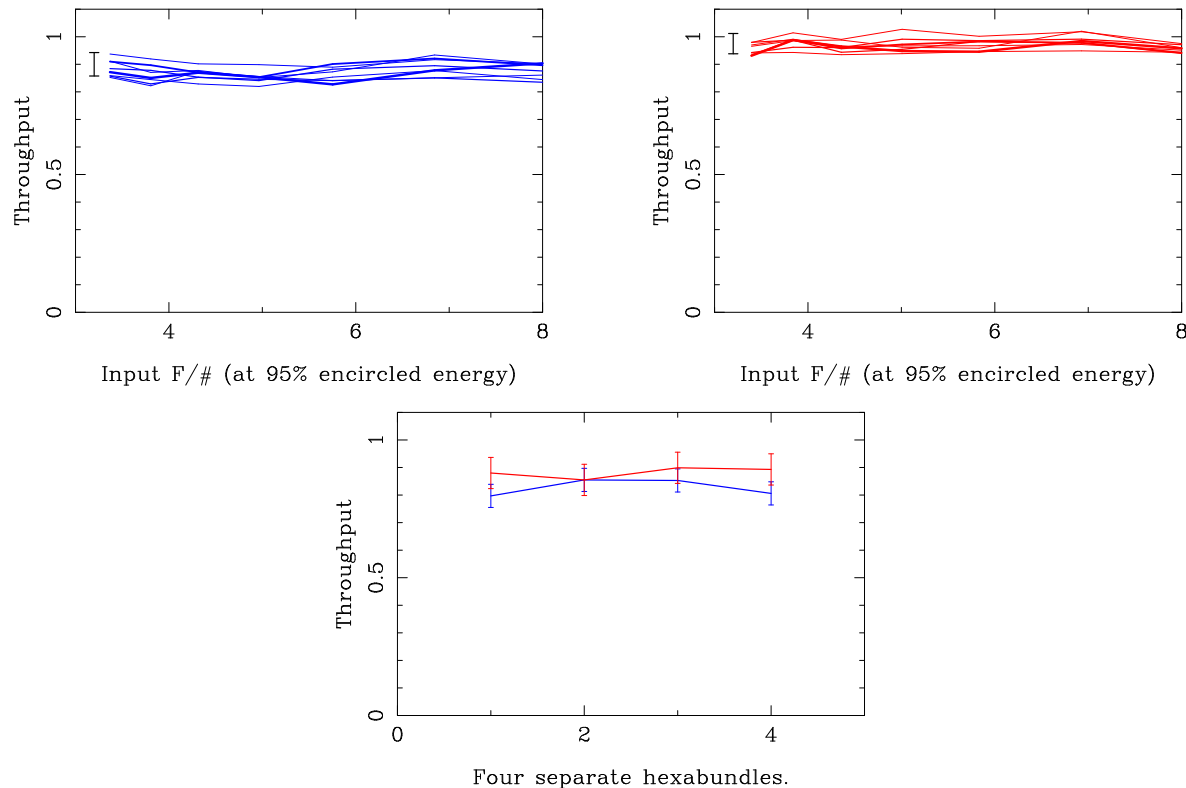


Figure 7. Input f-ratio (at 95% encircled energy) vs throughput of individual fibres. The top two plots show multiple fibres within one hexabundle, through the blue (left) and red (right) filters. Typical errors bars for each point are shown on the left side of each plot. The lower plot shows the throughput for a central fibre in four different hexabundles when the input was F/3.4. The red and blue lines are through those respective filters.

In order to test the trade-offs between fill-fraction and cross-talk, hexabundles have been made with a range of cladding thicknesses. For cladding thicknesses of $2\mu\text{m}$ or more, the cross-talk has been shown to be negligible compared to the effects of seeing, while delivering fill-fractions as high as 84%. FRD performance improves with decreasing f-ratio, and using the plots shown, the viability of any fibre system with a larger input f-ratio can be assessed from the FRD losses.

The early success of the hexabundle technology (Croom et al. 2012; Fogarty et al. 2012) has convinced us that this approach will come to dominate future large galaxy surveys.

Acknowledgements

We would like to thank Sergio Leon-Saval for useful discussions on topics surrounding this work.

This research was conducted by the Australian Research Council Centre of Excellence for All-sky Astrophysics (CAASTRO), through project number CE110001020.

REFERENCES

- Bland-Hawthorn J. et al., 2011, *Optics Express*, 19, 2649
 Bryant J. J., O’Byrne J. W., Bland-Hawthorn J., Leon-Saval S. G., 2011, *MNRAS*, 797
 Bryant J. J., et al., 2012a, *SPIE* 8446, 31
 Bryant J. J., Bland-Hawthorn J., 2012b *SPIE* 8446, 250
 Carrasco E., Parry I.R., 1994, *MNRAS*, 271, 1
 Crause L., Bershady M., Buckley D., 2008, *SPIE*, 7014, 210
 Croom S., et al., *MNRAS* 421, 872 (2012)
 Ellis S. C., Driver S. P., Allen P. D., Liske J., Bland-Hawthorn J., De Propris R., 2005, *MNRAS* 363, 1257
 Fogarty L. M. R. et al., 2012 *ApJ* 761, 169
 Gilbert J., et al., 2012, *SPIE* 8450, 14
 Gloge D., *Bell. Syst. Tech. J.*, 151, 1767 (1972)
 Haynes D. M., Withford M. J., Dawes J. M., Lawrence J. S., Haynes R., 2011, *MNRAS*, 414, 253
 Horton A. & Bland-Hawthorn J., 2007, *Op Ex*, 15, 1443
 Lawrence J., et al., 2012, *SPIE* 8446, 195
 Murphy J. D., MacQueen P. J., Hill G. J., Grupp F., Kelz A., Palunas P., Roth M., Fry A., 2008, *SPIE*, 7018, 92
 Oliveira A.C., de Oliveira L.S., dos Santos J.B., 2005, *MNRAS*, 356, 1079
 Poppett C. L., Allington-Smith J. R., 2010, *MNRAS*, 404, 1349
 Poppett C. L., Allington-Smith J. R., 2007, *MNRAS*, 379, 143
 Schmoll J., Roth M. M., Laux U., 2003, *PASP*, 115, 854
 Tody D., *Proc. SPIE* 627, 733 (1986)